Title

Evaluation of collapse resistance of reinforced masonry wall systems by shake-table tests

Journal

Earthquake Engineering & Structural Dynamics, 50(2)

ISSN

0098-8847

Authors

Cheng, Jianyu
Koutras, Andreas A
Shing, P Benson

Publication Date

2021-02-01

DOI

10.1002/eqe.3342

Peer reviewed

Received: 11 February 2020 | Revised: 11 August 2020 | Accepted: 13 August 2020

DOI: 10.1002/eqe.3342

WILEY

RESEARCH ARTICLE

Evaluation of collapse resistance of reinforced masonry wall systems by shake-table tests

Jianyu Cheng | **Andreas A. Koutras** | **P. Benson Shing**

Department of Structural Engineering, University of California, San Diego, La Jolla, California, USA

Correspondence
Jianyu Cheng, Department of Structural Engineering, University of California, San Diego, La Jolla, CA, USA.
Email: j7cheng@eng.ucsd.edu

Funding information
National Science Foundation (NSF), Grant/Award Number: CMMI-1728685

Summary

This paper presents a shake-table test study to investigate the displacement capacity of shear-dominated reinforced masonry wall systems and the influence of wall flanges and planar walls perpendicular to the direction of shaking (out-of-plane walls) on the seismic performance of a wall system. Two full-scale, single-story, fully grouted, reinforced masonry wall specimens were tested to the verge of collapse. Each specimen had two T-walls as the seismic force-resisting elements and a stiff roof diaphragm. The second specimen had six additional planar walls perpendicular to the direction of shaking. The two specimens reached maximum roof drift ratios of 17% and 13%, without collapsing. The high displacement capacities can be largely attributed to the presence of wall flanges and, for the second specimen, also the out-of-plane walls, which provided an alternative load path to carry the gravity load when the webs of the T-walls had been severely damaged. The second specimen developed a higher lateral resistance than the first owing to the additional axial compression exerted on the T-walls by the out-of-plane walls when the former rocked. The shear resistance of the T-walls evaluated with the design code formula matches the test result well when this additional axial compression is taken into account. However, it must be understood that the beneficial influence of the wall flanges depends on the magnitude of the gravity load because of the P-Δ effect and the severity of damage induced in the wall flanges when the wall system is subjected to bidirectional ground motions.

KEYWORDS

collapse resistance, displacement capacity, flanged walls, out-of-plane walls, reinforced masonry, shake-table test, shear walls, shear-dominated behavior

1 | INTRODUCTION

An accurate assessment of the displacement capacity of a building in an extreme earthquake event is of critical importance for life safety and collapse prevention. In ASCE/SEI 7-16,[1] the value of the seismic force modification factor (R) used in design has to ensure that the building has a low probability of collapse in the Maximum Considered Earthquake (MCE).[2] For reinforced masonry (RM) wall systems in high seismic areas, the value of the R factor is based on the notion that the walls can develop the necessary flexural ductility to sustain a certain amount of story drifts without collapsing when subjected to severe seismic forces. Nevertheless, in spite of the reinforcement and shear capacity design requirements in TMS 402/602[3] for RM walls designed for high seismic areas, such wall systems could still be susceptible

to shear-dominated behavior when there are wall components with a low shear–span ratio. This could be the case for perforated wall systems or when unintended coupling forces exerted by horizontal diaphragms significantly reduce the shear–span ratio of the walls.

The behaviors of RM planar wall segments dominated by flexure or shear were studied by a number of researchers.[4–11] The test results showed that the shear-dominated walls can develop a significantly lower displacement capacity than flexure-dominated walls. Although the above observations have raised concerns about the safety of buildings that may be susceptible to shear-dominated wall failures, the behavior of an RM building in a severe earthquake event depends on a number of factors, such as the overstrength and the influence of other structural elements and their interaction with RM shear walls, which could be beneficial or detrimental to the seismic performance of the building. Moreover, RM buildings often have flanged walls. The influence of wall flanges on the behavior of walls dominated by diagonal shear cracks is not well understood. Limited studies were carried out to investigate the seismic performance of RM flanged walls. He and Priestley[12] conducted cyclic quasi-static tests and shake-table tests to study the behavior of flexure-dominated RM T-walls. However, there are no experimental data available on the shear-dominated behavior of flanged RM walls.

Experimental studies were carried out to investigate the seismic performance of fully grouted RM wall systems. Merryman et al.[13] performed cyclic quasi-static tests on 2 two-story coupled RM wall systems with different horizontal diagrams and different levels of vertical loads. Seible et al.[14] tested a five-story RM building with the pseudo-dynamic test method. The walls were dominated by flexure exhibiting little load degradation. Heerema et al.[15] and Ashour et al.[16] performed quasi-static tests on two scaled, two-story, RM wall systems that had the same wall layouts but different diaphragm designs. The system with the more flexible diaphragms[15] reached a roof drift ratio of 2.5% with 38% loss in the lateral resistance. The system with the stronger diaphragms[16] showed 50% higher peak lateral resistance but more brittle behavior with 72% strength degradation at a roof drift ratio of 2.5%. Mavros et al.[17] and Stavridis et al.[18] conducted shake-table tests to study the seismic behavior of RM wall systems with shear-dominated wall components. The two-story wall system tested by Mavros et al.[17] showed a 20% strength degradation at a maximum first-story drift ratio of 2%. Similarly, the three-story structure tested by Stavridis et al.[18] had a 27% strength degradation at a maximum first-story drift of 1.6%. The displacement capacity observed in these shake-table tests[17,18] is significantly higher than that of shear-dominated planar wall segments tested by Voon and Ingham,[8] Shing et al.,[9,10] and Ahmadi,[11] which exhibited severe load degradations at drift ratios not exceeding 1%. The more ductile behavior observed in the wall systems in these shake-table tests[17,18] could be attributed to the presence of wall flanges as well as displacement histories. However, the exact influence of the wall flanges is not well understood. In all the aforementioned studies, the maximum inter-story drift that an RM wall system could reach before collapse was not attained because the tests were stopped way before the collapse point.

There are limited test data on the collapse or near-collapse behavior of masonry wall structures. Tomaževič and Weiss[19] tested two 1:5-scale, three-story building models on a shake table. One had plain masonry, and the other had wire reinforcement placed along the vertical edges of each wall, as well as the wire stirrups distributed horizontally. Whereas the plain masonry structure collapsed at a first-story drift ratio of 2.5%, the RM structure was able to reach a first-story drift of nearly 4% without collapse. Lourenço et al.[20] tested two 1:2-scale concrete masonry building models on a shake table. The first model was unreinforced, and the second one had truss-type steel reinforcement distributed vertically and horizontally in each wall. Both structures had two stories and were subjected to bidirectional base excitation. In the tests, the unreinforced model collapsed when reaching a maximum interstory drift ratio of 2.5% at the second story. However, the model with truss-type reinforcement reached a maximum inter-story drift of 0.34% at the first story without collapse when the intensity of the base excitation was 60% stronger than that of the last excitation applied to the unreinforced model. Koutras and Shing[21] investigated the behavior of a single-story partially grouted RM structure that was designed for a low-to-moderate seismic zone based on TMS 402/602.[3] The structure was tested on a shake table under a sequence of unidirectional motions until it was severely damaged. In the tests, the structure lost 85% of its lateral strength at a drift ratio of 2.2%. Collapse was averted only because the walls perpendicular to the direction of shaking were able to carry the weight of the roof after the walls parallel to motion had been severely damaged. However, no test data are available on the behavior of fully grouted RM shear wall systems near collapse.

This paper presents a study to investigate the displacement capacity of shear-dominated fully grouted RM wall systems and the influence of wall flanges and planar walls perpendicular to the direction of the seismic force on the seismic performance of a wall system. To this end, two full-scale, single-story, RM wall systems were tested on a shake table to the verge of collapse. The tests were carried out with unidirectional base excitation. The paper presents the design of the two structures, the testing procedure, and the major results and findings from the shake-table tests. The

influence of wall flanges and walls perpendicular to the direction of shaking has been analyzed and quantitatively assessed. The responses of the test structures have been compared with a force–drift ratio backbone curve developed from previous quasi-static test data on shear-dominated planar wall segments.[22] The results have been further used to assess the accuracy of the shear strength formula in TMS 402/602.[3] The test data were also useful for validating computational models that were used to assess the collapse vulnerability of RM building systems.[23]

2 | DESIGN OF TEST STRUCTURES

Figure 1 shows the plan layouts of the two RM shear wall systems designed and tested under unidirectional motions on the outdoor shake table in the NHERI (Natural Hazards Engineering Research Infrastructure) facility at the University of California, San Diego. Each specimen had two T-walls as the main seismic force-resisting system. Specimen 2 had six additional rectangular walls with their planes oriented perpendicular to the direction of the shake-table motion. They are referred to as the out-of-plane walls in this paper. One of the objectives of the tests was to investigate the influence of the out-of-plane walls on the seismic resistance of a wall system. To this end, the T-walls in the two specimens had the same design and carried the same gravity load, and the two specimens had the same effective seismic weight.

Figure 2 shows the reinforcement details for the two specimens. The reinforcing bars in the walls had a nominal yield strength of 414 MPa (Grade 60 in ASTM standard[24]). Each T-wall had six No. 4 (13 mm) vertical bars spaced at 20 cm (8 in.) on center in the web, and three No. 4 (13 mm) vertical bars spaced at 41 cm (16 in.) in the flange. The horizontal bars in the web and the flange were No. 3's (10 mm) spaced at 41 cm (16 in.) on center. In Specimen 2, each of the out-of-plane walls had No. 4 (13 mm) bars for the vertical reinforcement and No. 3 (10 mm) bars for the horizontal reinforcement, both spaced at 41 cm (16 in.) on the center. The reinforcement complied with the prescriptive requirements of TMS 402/602[3] for walls designed for high seismic areas, but the spacing of the reinforcing bars in the flanges of the T-walls slightly violated the maximum spacing requirement (which is no greater than one third of the wall length). The vertical reinforcement ran continuously from the walls into the footings, and each bar ended with a 90° standard hook in the footing conforming to the ACI 318-14 specification[25] for the development of reinforcement in tension. The surface of the concrete footing underneath each wall was intentionally roughened to increase the frictional resistance.

As shown in Figure 2, the roof slab of Specimen 1 consisted of 25-cm-thick (10-in.) precast prestressed hollow-core planks with a 13-cm-thick (5-in.) cast-in-place concrete topping. Two reinforced concrete slabs, each with dimensions of 3.0 × 3.0 × 0.36 m (10 ft × 10 ft × 14 in.), were secured on top of the roof slab to achieve the target roof mass. For Specimen 2, the roof slab consisted of 20-cm-thick (8-in.) hollow-core planks with a 7.6-cm (3-in.) concrete topping. It had four additional concrete slabs, each with dimensions of 5.0 × 3.0 × 0.25 m (16.5 ft × 10 ft × 10 in.), as added mass. The resulting roof weights of Specimens 1 and 2, including the added concrete slabs, were 245 kN (55.1 kips) and 601 kN (135 kips), respectively. The roof weights of the two specimens were so determined that the T-walls in the two specimens carried the same gravity load. Because the roof slabs were very stiff, the tributary roof load, P, on each wall was assumed to be proportional to the axial stiffness of the wall. The axial compressive load ratio, P/f'_mA_g, for each T-wall was 0.016, where A_g is the cross-sectional area of the wall. The compressive strength of masonry, f'_m, was specified to be 17 MPa (2.5 ksi). Including the weight of the masonry walls from the mid-height to the top, Specimen 1 had an

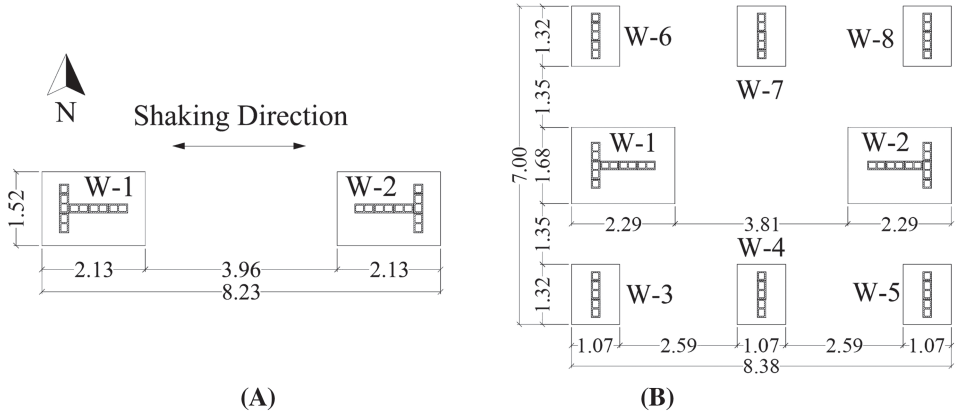

FIGURE 1 Plan views of footing and wall layout (in meters): A, Specimen 1; B, Specimen 2

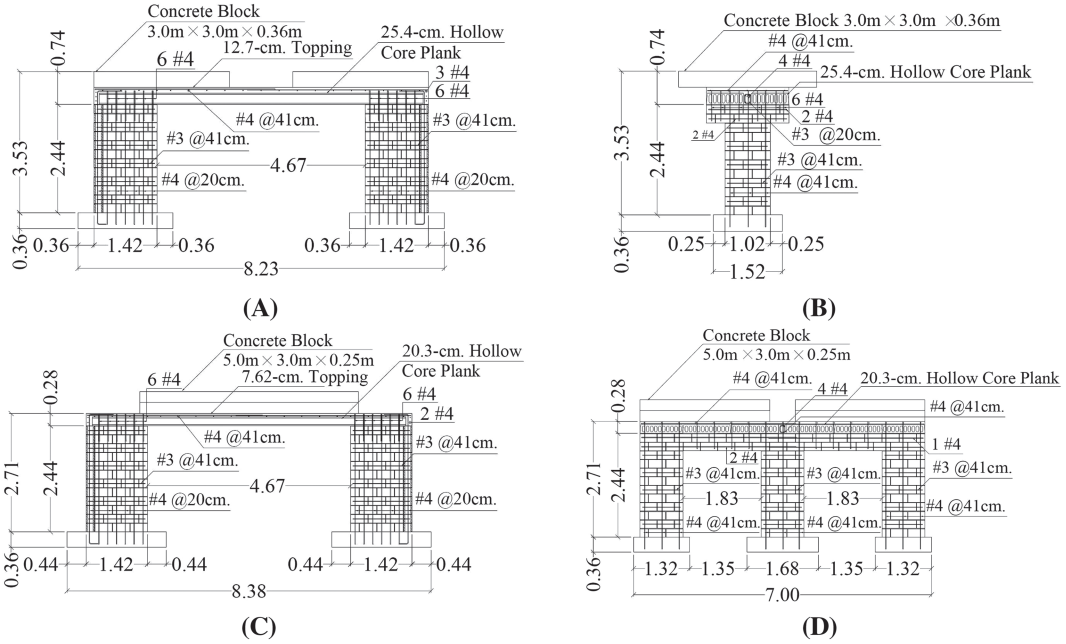

FIGURE 2 Reinforcement details (in meters unless indicated): A, south elevation view of Specimen 1; B, west elevation view of Specimen 1; C, south elevation view of T-walls in Specimen 2; D, west elevation view of Specimen 2

actual seismic weight of 268 kN (60 kips), while Specimen 2 had 661 kN (149 kips). To have the same effective seismic weight as Specimen 2, the input ground motions for Specimen 1 were scaled in time and amplitude to meet the dynamic similitude requirement.

The flexural, diagonal shear, and sliding shear strengths of the T-walls were calculated based on the recommendations and formulas in TMS 402/602[3] to ensure that the walls would develop diagonal shear-dominated behavior. The flexural strength was calculated using an axial force–moment interaction diagram. It was assumed that the T-walls had a fixed–fixed end condition due to the high stiffness of the roof diaphragms. The calculated flexural, diagonal shear, and sliding shear strengths were 355 kN (80 kips), 326 kN (73 kips), and 397 kN (89 kips), respectively, based on the masonry compressive strength of 17 MPa (2.5 ksi) and the expected yield strength of 469 MPa (68 ksi) for the reinforcing bars. A detailed finite element model was used to conduct pre-test analysis to determine the ground motion intensity scaling in the shake-table tests as discussed in a following section.[23]

3 | MATERIAL PROPERTIES

For both specimens, compression tests were performed on 203 × 102 × 102-mm (8 × 4 × 4-in.) grout prisms, 406 × 203 × 203-mm (16 × 8 × 8-in.) grouted CMU prisms, and 152 × 305-mm (6 × 12-in.) concrete cylinders. For Specimen 2, compression tests were also performed on 102 × 203-mm (4 × 8-in.) grout cylinders and 51 × 102-mm (2 × 4-in.) mortar cylinders. The compression tests were conducted on the 28th day after the samples were prepared, and some samples were also tested several days after the first ground motion test was performed. The average compressive strengths of the masonry and concrete samples are shown in Table 1. Tension tests were conducted on reinforcing bar samples. The average tensile properties are presented in Table 2.

4 | INSTRUMENTATION

Each specimen had a number of sensors installed to measure the response of the structure during the tests. Specimen 1 had 76 strain gauges, 24 accelerometers, and 56 displacement transducers. Specimen 2 had 136 strain gauges, 40 accelerometers, and 69 displacement transducers. Figure 3 shows the locations of the accelerometers and displacement transducers installed on the two specimens. Some locations had a set of three accelerometers to measure the

TABLE 1 Compressive strengths of masonry and concrete samples

Specimen	Type of samples	Age (days)	Number of samples	Compressive strength		
				Average		
				MPa	ksi	COV
1	406 × 203 × 203-mm grouted CMU prisms	28	2	18	2.7	0.06
		68[b]	6	20	2.9	0.13
	203 × 102 × 102-mm grout prisms	28	2	27	3.9	0.01
		68[b]	3	32	4.7	0.02
	152 × 305-mm footing concrete cylinders	28	3	36	5.2	0.03
	152 × 305-mm roof concrete cylinders	28	3	35	5.0	0.02
2	406 × 203 × 203-mm grouted CMU prisms	28	7	27	3.9	0.07
	203 × 102 × 102-mm grout prisms	28	3	36	5.2	0.07
		70[c]	5	45	6.5	0.23
	102 × 203-mm grout cylinders	28	3	33	4.8	0.04
		70[c]	3	37	5.3	0.02
	51 × 102-mm mortar cylinders[a]	28	12	30	4.4	0.12
	152 × 305-mm footing concrete cylinders	28	3	36	5.3	0.03
	152 × 305-mm roof concrete cylinders	28	3	43	6.3	0.03

[a]Three batches with four samples in each batch.
[b]Six days after the first ground motion test on Specimen 1.
[c]Eight days after the first ground motion test on Specimen 2.

TABLE 2 Average tensile properties of reinforcing bars

Specimen	Bar size	Number of samples	Yield stress		Tensile strength		ϵ_y [a]	ϵ_{sh} [b]	ϵ_{su} [c]
			MPa	ksi	MPa	ksi	mm/mm (in./in.)	mm/mm (in./in.)	mm/mm (in./in.)
1	No. 3	3	521	75.6	729	105.8	0.00474	-	0.107
	No. 4	3	462	67.0	671	97.3	0.00342	0.0106	0.116
2	No. 3	3	523	75.9	730	105.9	0.00495	-	0.107
	No. 4	3	461	66.9	671	97.3	0.00339	0.0107	0.117

[a]Yield strain.
[b]Strain at initiation of strain hardening.
[c]Strain at peak stress.

acceleration in east–west, north–south, and vertical directions, respectively. For Specimen 1, a set of three accelerometers was located at each corner of the roof slab. Eight sets of accelerometers were installed along the roof perimeter of Specimen 2. To record the table acceleration during the tests, four sets of accelerometers were installed on the top surfaces of the concrete footings of the T-walls in both specimens.

For both specimens, there were seven string potentiometers installed on the north face of the web of each T-wall to measure the wall deformation. As shown in Figure 3A,B, on the east and west sides of a T-wall, a string potentiometer was installed to measure the vertical displacement of the roof slab. For Specimen 2, one string potentiometer was installed along the center line of each out-of-plane wall to measure the vertical roof displacement, as shown in Figure 3D–F. The horizontal displacement of the roof relative to the table (the story drift) was measured by string potentiometers mounted along the east edge of the roof with the ends of the strings attached to a stiff reference frame, which was fixed on the table. As shown in Figure 3B,F, Specimen 1 had two string potentiometers to measure the relative roof displacement, and Specimen 2 had three. The multiple string potentiometers were to check if there was

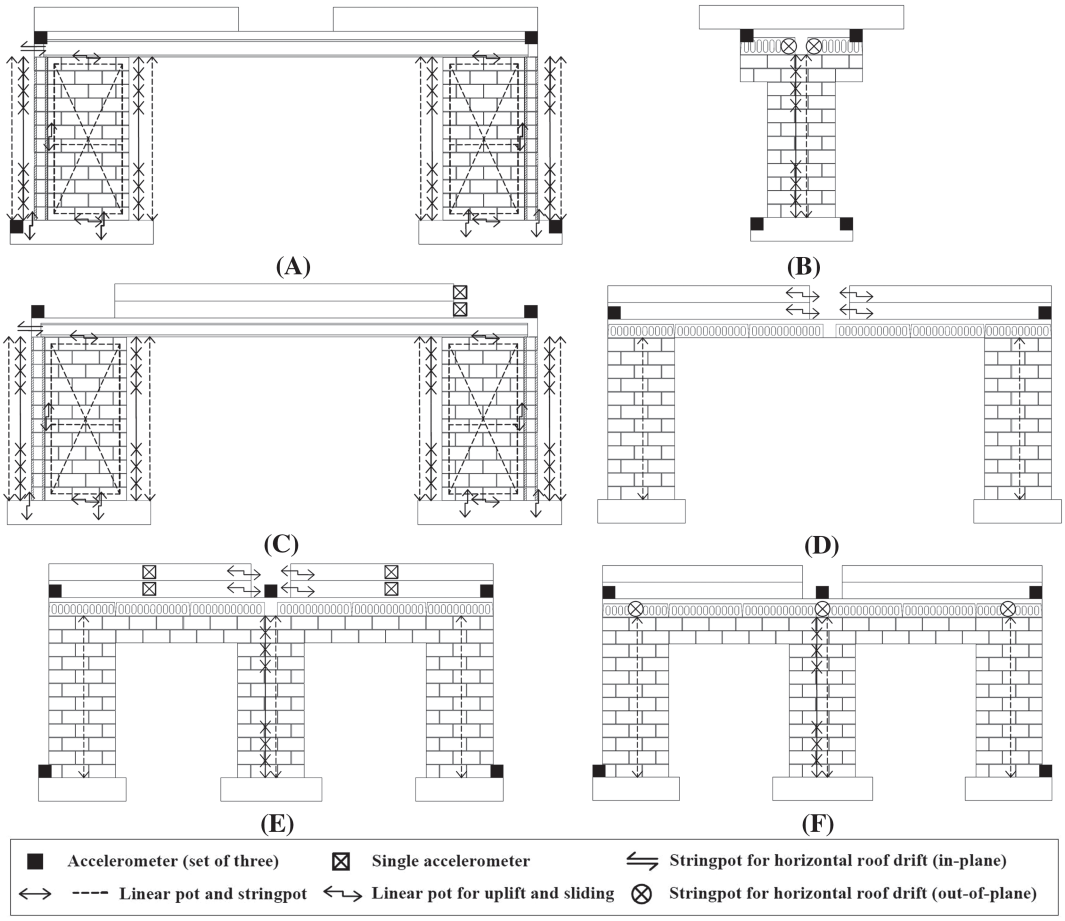

FIGURE 3 Instrumentation plans for Specimens 1 and 2: A, north view of Specimen 1; B, east view of Specimen 1; C, north view of two T-walls in Specimen 2; D, west view of two central out-of-plane walls in Specimen 2; E, west view of Specimen 2; F, east view of Specimen 2

horizontal rotation of the roof. Figure 3A,C also shows that 14 linear potentiometers were installed on the east and west sides of each T-wall to measure the flexural deformation (seven potentiometers on each side). The remaining linear potentiometers were used to measure the uplift and sliding of the base of each T-wall relative to the footing, the sliding between the top of each wall and the roof slab, and the sliding between the web and the flange if any.

For Specimen 2, sensors were installed to check if the concrete blocks secured on the roof slab slid during the tests. They included an accelerometer (along the shaking direction) attached to the west vertical surface of each block and linear potentiometers installed to measure the relative sliding between the roof top and the lower concrete block, and between two stacked blocks.

Strain gauges were installed on the vertical bars near the top and bottom of each wall to measure the flexural strains. Additional gauges were installed on vertical and horizontal bars in the webs of the T-walls along diagonal lines to measure strains induced by diagonal crack opening. The locations of the strain gauges will be shown later in Figures 14 and 15 together with the detected yielding.

5 | TEST SETUP AND LOADING PROTOCOL

Figure 4 shows the two specimens with their footings secured on the shake table with post-tensioned rods. The table motion was in the east–west direction. For each specimen, four concrete pedestals, with two on each of the north and south sides, were used as a catch system to prevent the free fall of the roof slab onto the table in case the walls lost their vertical load carrying capacity. Four steel cables were used to tie the roof slab to the table platen with a slack to avoid uncontrolled drift of the roof. Specimen 1 was tested in two phases. In the first phase, the structure was subjected to a

sequence of earthquake motions until it reached a roof drift ratio of 2.53% with a significant strength degradation at the end. In the second phase, the damaged structure was subjected to a quasi-static lateral load with the test setup shown in Figure 5. Two cables were used to pull the roof slab by moving the table away from a stiff steel reaction tower, to which the other ends of the cables were attached. During the quasi-static test, the lateral load was monitored with two load cells. The horizontal roof displacement was increased until the lateral resistance of the tested structure dropped close to zero. Specimen 2 was tested with a sequence of ground motions until the structure was on the verge of collapse.

Two ground motion records from the 1994 Northridge Earthquake were selected for the shake-table tests: a far-field record from the Mulholland station (abbreviated as MUL below) and a near-fault record from the Rinaldi station (abbreviated as RIN below). Table 3 shows the sequences of input ground motions applied to the two specimens. After each earthquake motion, the specimen was subjected to white-noise excitation to identify any change in its natural period. The white noise had a root-mean-square amplitude of 0.03 g and a duration of 3 min. The fundamental periods of both specimens before and after each motion are shown in Table 3. For Specimen 1, only the Mulholland record was used, with the acceleration scaled to 45%, 90%, 120%, and 133% of that of the original record in seven runs. For Specimen 2, the Mulholland record was used in the first six runs, with the acceleration scaled to 45%, 90%, 120%, 133%, and 160% of that of the original record. For the last run, the Rinaldi record was used with an intensity scaling of 130%. The Rinaldi record was selected for the last run because the fundamental period of the structure showed a significant elongation (to 0.328 s) after the sixth run, and the acceleration response spectrum of the record has a more or less uniform amplitude in the period range of 0.3 to 0.7 s, as shown in Figure 6A. Moreover, as shown in Figure 6C, the long-duration pulse in the acceleration time history of the Rinaldi record would induce a large displacement demand.

Because Specimens 1 and 2 had different roof weights, as mentioned before, additional scaling was applied to the time and amplitude of the earthquake records used for Specimen 1 to attain the dynamic similitude between the two specimens. The ground acceleration was scaled up by a factor of $S_a = 2.4$ (seismic weight of Specimen 2/seismic weight of Specimen 1), and the time was compressed by a factor of $\sqrt{1/S_a} = 0.65$, with the assumption that both structures had the same lateral stiffness and strength as would be the case in design practice. The value of S_a was calculated with the seismic weights estimated prior to the construction of the specimens, and it was 2.7% lower than the value calculated with the actual weights. Figure 6B shows the table acceleration histories for the 90%-level Mulholland records obtained from two tests performed on Specimens 1 and 2, respectively.

6 | GENERAL TEST OBSERVATIONS AND GLOBAL RESPONSES

This section presents the major observations and the structural response obtained from the tests of the two specimens. Table 4 summarizes the behaviors of the two test specimens. The peak values of the roof drift ratio, base shear, and base sliding occurring at different ground motion levels are summarized in Table 5. The positive direction for the displacement response is towards the east, as defined in Figure 1. The roof drift ratio was calculated as the relative roof displacement divided by the wall height of 2.44 m (8 ft). The base shear was calculated as the product of the average roof acceleration along the shaking direction, measured by the accelerometers installed on the roof slab, and the seismic mass consisted of the total roof mass and the masonry mass above the mid-height of the walls. As shown in Table 3, Specimen 1 had an initial fundamental period of 0.072 s, while Specimen 2 had an initial period of 0.090 s. However, with the consideration of the time scale factor of 0.65 applied to Specimen 1 to satisfy the dynamic similitude with Specimen 2, the actual initial period of Specimen 1 was 0.111 s. Specimen 2 had a shorter period than Specimen 1. This

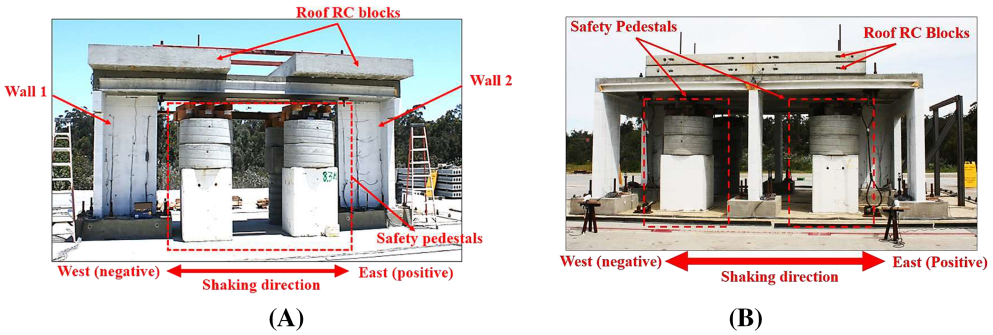

FIGURE 4 Shake-table test setups: A, Specimen 1; B, Specimen 2

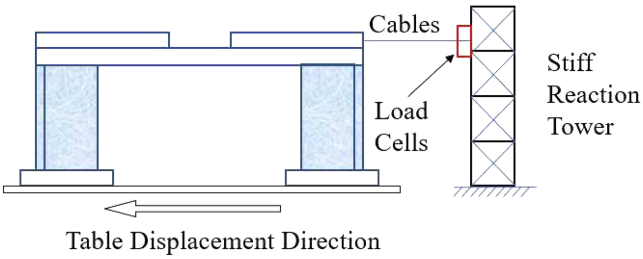

FIGURE 5 Pull test setup for Specimen 1

TABLE 3 Test sequences for Specimens 1 and 2

Specimen 1			Specimen 2		
Test ID	**Input motion**	**Period after test (s)**	**Test ID**	**Input motion**	**Period after test (s)**
Initial	N/A	0.072	Initial	N/A	0.090
1	MUL-45%	0.072	1	MUL-45%	0.090
2	MUL-45%	0.074	2	MUL-90%	0.097
3	MUL-90%	0.090	3	MUL-120%	0.121
4	MUL-90%	0.095	4	MUL-90%	0.123
5	MUL-90%	0.107	5	MUL-133%	0.164
6	MUL-120%	0.166	6	MUL-160%	0.328
7	MUL-133%	0.751	7	RIN-130%[a]	-
8	Static pull[a]	-			

[a]No white-noise test was performed because of the damage state of the specimens.

could be attributed to the higher initial stiffness of Specimen 2 because of the out-of-plane wall components. Observations for each specimen in the tests are described below with the wall numbers identified in Figure 1.

6.1 | Specimen 1

6.1.1 | Tests up to MUL-90%

Two low-intensity and three mid-intensity tests were conducted on Specimen 1 by scaling the Mulholland record to 45% and 90%, respectively. The two low-intensity motions and the first mid-intensity motion were to check the instrumentation. No visible cracks were observed on the walls during the two 45%-level motions. As shown in Table 3, the fundamental period of the intact specimen (0.072 s) hardly changed after these shakings. After the first shaking with the 90% level motion, the fundamental period of the specimen increased by 0.018 s, indicating that some damage had occurred during the test. After three shakings with the 90%-level motions, it was observed that a few hairline flexural cracks initiated in the webs near the bottom of the two walls. The fundamental period measured from the white-noise tests increased to 0.107 s.

6.1.2 | Test with MUL-120%

During the test with the 120%-level Mulholland motion, hairline cracks occurring in the last few tests opened and extended. Meanwhile, more flexural cracks initiated and propagated in the webs and flanges near the bottom of both walls, as shown in Figure 7. The fundamental period of the specimen increased from 0.107 to 0.166 s, which was largely attributed to the development of flexural cracks and the yielding of the vertical reinforcement near the wall base. Figure 8A shows the global response of the structure during this motion.The maximum resistance developed by the structure reached 598 kN (134 kips) at a roof drift ratio of 0.35%. The maximum roof drift ratio reached in this test was 0.47%.

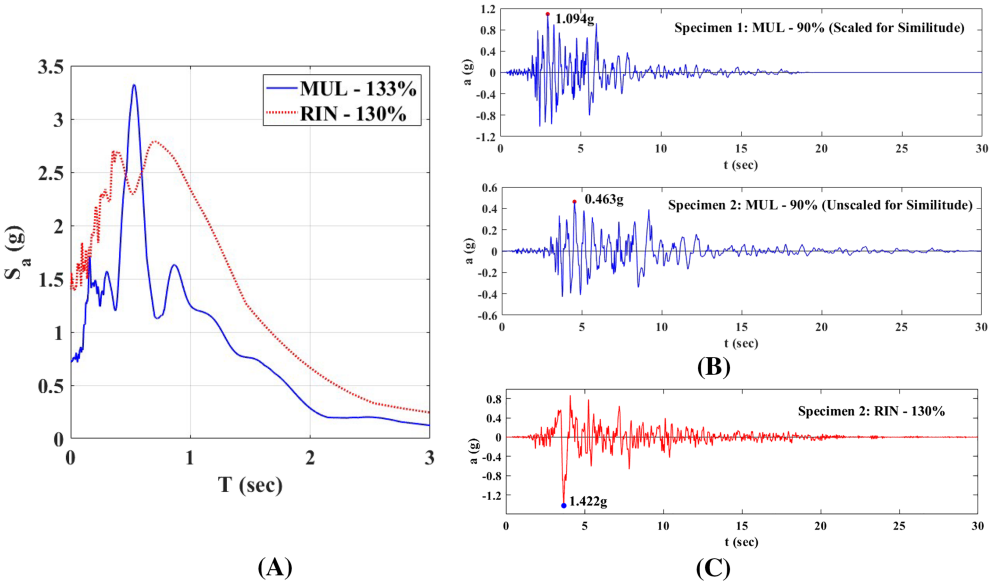

FIGURE 6 Table motions recorded in shake-table tests: A, acceleration spectra of MUL-133% and RIN-130% from the tests of Specimen 2; B, Acceleration histories for MUL-90% from the tests of Specimens 1 and 2; C, Acceleration history for RIN-130% from the test of Specimen 2

TABLE 4 Summary of test specimen behaviors

Spec.	Failure mode	Maximum lateral resistance: Test value V_{max} (kN)	Maximum lateral resistance: Code formula[a] V_n (kN)	V_{max}/V_n	Max. roof drift (%)	Occurrence of collapse	Strength degradation at different roof drift levels (%): 2% drift	5% drift	10% drift
1	Shear	689	685	1.00	16.7	No	18.3	43.5	72.3
2	Shear	925	783	1.18	13.4	No	19.4	45.9	78.4

[a]The shear strength formulation in TMS 402/602 (TMS 2016).

TABLE 5 Peak values of structural responses for select ground motions

Spec.	Test ID	Input motion	Peak roof displacement (cm): Pos.	Peak roof displacement (cm): Neg.	Peak roof drift[a] (%): Pos.	Peak roof drift[a] (%): Neg.	Peak base shear (kN): Pos.	Peak base shear (kN): Neg.	Peak base sliding at Wall 1 (mm): Pos.	Peak base sliding at Wall 1 (mm): Neg.	Peak base sliding at Wall 2 (mm): Pos.	Peak base sliding at Wall 2 (mm): Neg.
1	5	MUL-90%	0.56	0.49	0.23	0.20	469	472	0.17	0.24	0.48	0.45
	6	MUL-120%	1.01	1.14	0.42	0.47	598	561	0.37	0.50	1.00	1.01
	7	MUL-133%	5.05	6.15	2.07	2.52	619	690	0.56	1.19	1.70	2.78
	8	Static Pull[b]	40.7	-	16.7	-	394	-	-	-	-	-
2	2	MUL-90%	0.19	0.16	0.08	0.06	414	432	0.14	0.04	0.11	0.04
	3	MUL-120%	0.29	0.35	0.12	0.14	521	598	0.34	0.25	0.35	0.21
	5	MUL-133%	0.41	0.61	0.17	0.25	618	722	0.68	0.70	0.76	0.59
	6	MUL-160%	1.18	2.20	0.48	0.90	777	925	2.21	3.00	2.63	2.58
	7	RIN-130%	32.7	22.1	13.4	9.07	902	428	3.77	4.98	2.42	8.10

[a]Roof drift ratios are calculated based on a wall height of 2.44 m.
[b]Test 8 was a quasi-static test in which all displacement transducers measuring base sliding were removed.

6.1.3 | Test with MUL-133%

The last dynamic test on Specimen 1 was conducted with a 133%-level Mulholland motion. In this test, the walls developed severe shear cracks. The specimen exhibited significant lateral drifts as the period of the structure elongated into

the range in which the acceleration spectrum of the record peaked. The damage shifted the fundamental period of the structure from 0.166 to 0.751 s, as shown in Table 3, with the peak spectral acceleration of the ground motion occurring at 0.35 s after the similitude scaling. Figure 9 shows the severe diagonal shear cracks and the masonry spalling and crushing that developed in the webs of the T-walls. However, none of the diagonal cracks propagated into the flanges. As shown in Figure 9B, Wall 2 (East T-Wall) also showed base crushing and subsequent buckling of the extreme vertical bar in the web near the wall base. The base shear–roof drift hysteresis curves for the structure (Figure 8) show that the peak strength of 690 kN (155 kips) was reached at a roof drift ratio of about 1% in the negative (west) direction. A maximum roof drift ratio of 2.53% was reached in the west direction. At this drift level, the lateral resistance of the tested structure dropped to 340 kN (76.3 kips), which was about 50% of the peak strength.

6.1.4 | Quasi-static pull test

After MUL-133%, to examine the maximum roof drift ratio that could be sustained by the structure before collapse, a quasi-static test was conducted by pulling the roof with steel cables. The quasi-static test was done instead of a dynamic test because of safety reasons. During the quasi-static test, the diagonal cracks in each wall continued to extend and open as the horizontal roof displacement increased. Severe crushing and spalling of the masonry were observed. As shown in Figure 8B, the lateral resistance of the wall system dropped to 44 kN (9.9 kips), which is 6% of the peak strength, when a roof drift ratio of 16.7% (42.4-cm roof horizontal displacement) was reached. Horizontal cracks were observed in the wall flanges, and a few diagonal cracks in the webs had extended into the flanges. As shown in Figure 10, at the roof drift ratio level of 16.7%, collapse was averted because the flanges were still able to carry the weight of the roof slab when the masonry in the wall webs had been severely crushed.

6.2 | Specimen 2

6.2.1 | Tests up to MUL-133%

Specimen 2 was subjected to a similar sequence of ground motions as Specimen 1, which were 45%-, 90%-, 120%-, and 133%-level Mulholland motions, as shown in Table 3. An additional MUL-90% motion (test No. 4) was applied after the MUL-120% motion to check the instrumentation after the replacement of two faulty accelerometers. Whereas flexural

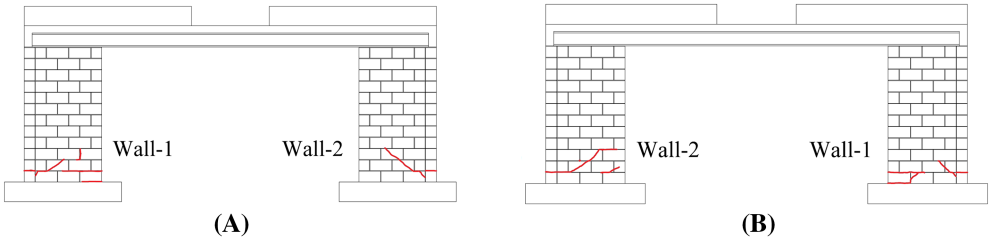

FIGURE 7 Crack patterns on Specimens 1 after MUL-120%: A, south view; B, north view [Colour figure can be viewed at wileyonlinelibrary.com]

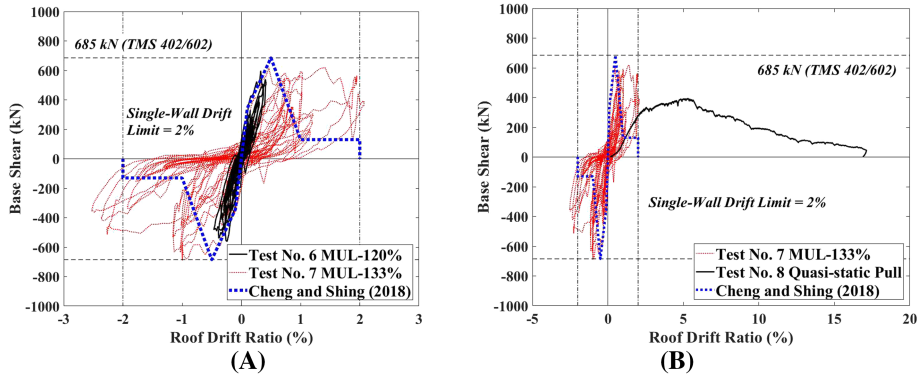

FIGURE 8 Base shear–roof drift ratio curves for Specimen 1: A, responses from the ground motion tests; B, results from the quasi-static and last ground motion tests [Colour figure can be viewed at wileyonlinelibrary.com]

and shear cracks developed in Specimen 1 after the 120%- and 133%-level Mulholland motions, there were no visible cracks observed in Specimen 2 after the MUL-133%. The fundamental period of Specimen 2 increased slightly from 0.090 to 0.097 s after the first MUL-90%.

Figure 11A shows the base shear–roof drift ratio curves for the 120%- and 133%-level Mulholland motions applied to Specimen 2. During the test with MUL-120%, the specimen reached a maximum base shear of 598 kN (135 kips) at a drift ratio of 0.14%. The fundamental period increased to 0.121 s after this motion and remained unchanged after the following MUL-90%. Figure 11A also shows that the specimen developed nonlinearity during MUL-133%. The peak drift ratio reached in the test was 0.25%, whereas the maximum base shear developed was 726 kN (163 kips). The period of the specimen increased to 0.164 s, indicating some damage.

6.2.2 | Test with MUL-160%

During MUL-160%, the period of the specimen elongated from 0.164 to 0.328 s. A maximum drift ratio of 0.90% was reached. As shown in Figure 11, the base shear capacity of 925 kN (208 kips) was reached at a roof drift ratio of 0.60% in the negative (west) direction. During the test, load degradation was relatively mild, about 22% with respect to the peak. Figure 12 shows the crack pattern obtained after MUL-160%. Flexural and diagonal shear cracks occurred in the webs of the T-walls. As shown in Figure 12A, in the web of Wall 1, a major diagonal crack extended from the top right corner to the wall flange above the fourth course of masonry units from the base and then propagated as a horizontal crack in the flange. On the same wall, a crack developed along the flange–web interface, propagating from the end of the major diagonal crack down to the wall base. In Wall 2, major diagonal cracks extended into the toe of the web at one end and to the flange at an approximately 60° angle with respect to the horizontal at the other, propagating vertically up along the web-flange interface. Similar to Wall 1, one diagonal crack extended into the wall flange and formed a horizontal crack on the flange. Furthermore, several flexural cracks initiated and propagated in the lower part of the wall webs. Toe crushing occurred in the web of Wall 2. As shown in Figure 12C,D, horizontal cracks developed at the top of the out-of-plane walls right below the lintel. For the two middle out-of-plane walls (Walls 4 and 7 as identified in Figure 1), no visible cracks were observed.

FIGURE 10 Damage in Specimen 1 after the quasi-static pull test [Colour figure can be viewed at wileyonlinelibrary.com]

(A) (B)

FIGURE 9 Damage in Specimen 1 after MUL-133%: A, south view of Wall 1; B, north view of Wall 2

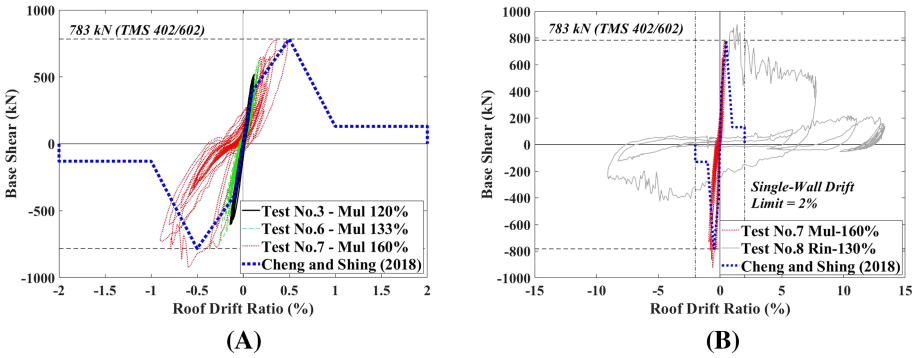

FIGURE 11 Base shear–roof drift ratio curves for Specimen 2: A, Mulholland motions; B, last two motions [Colour figure can be viewed at wileyonlinelibrary.com]

6.2.3 | Test with RIN-130%

During RIN-130%, the T-walls developed severe damage. A maximum drift ratio of 13.4% was reached, but the structure did not collapse. The base shear–roof drift ratio curves in Figure 11B show that the maximum base shear reached 902 kN (203 kips) at a drift ratio of 1.39% in the positive (east) direction. The specimen developed a residual strength of 185 kN (41.6 kips), which was about 20% of the peak strength (208 kips) reached during MUL-160%. Figure 13 shows the damage of the specimen after the test. The diagonal cracks developed during MUL-160% extended further and were accompanied by the opening of new diagonal cracks in the webs of the T-walls. As in the quasi-static test of Specimen 1, severe masonry crushing occurred in the wall webs. The webs and flanges of the T-walls were practically separated. The failure of the 90° hooks connecting the flanges and webs was observed, along with the fracture of the horizontal bars crossing the flange–web interfaces. The flanges of the T-walls exhibited severe out-of-plane bending at the elevation of the horizontal cracks that developed in motion MUL-160%. Figure 13E shows that masonry spalling occurred on the east face of Specimen 2. Moreover, cracks radiated from the corners between the lintels and the out-of-plane rectangular walls, as shown in Figure 13B,F. However, the roof slab remained practically intact during the test.

7 | ANALYSIS OF TEST RESULTS

7.1 | Yielding and fracture of reinforcing bars

Figures 14 and 15 show the sequence of yielding in the reinforcing bars in Specimens 1 and 2, respectively. Yielding in the reinforcing bars was determined by comparing the average yield strain obtained in the material sample tests and the strains recorded by the strain gauges attached to the bars.

The first yielding in Specimen 1 occurred during the first MUL-90% (test No. 3) motion. The vertical bars at the two extreme sides of the two T-walls yielded in tension near the wall base, as shown in Figure 14. After three shakings with MUL-90%, three (out of six) vertical bars in the flanges had yielded at the first masonry course from the base. Moreover,

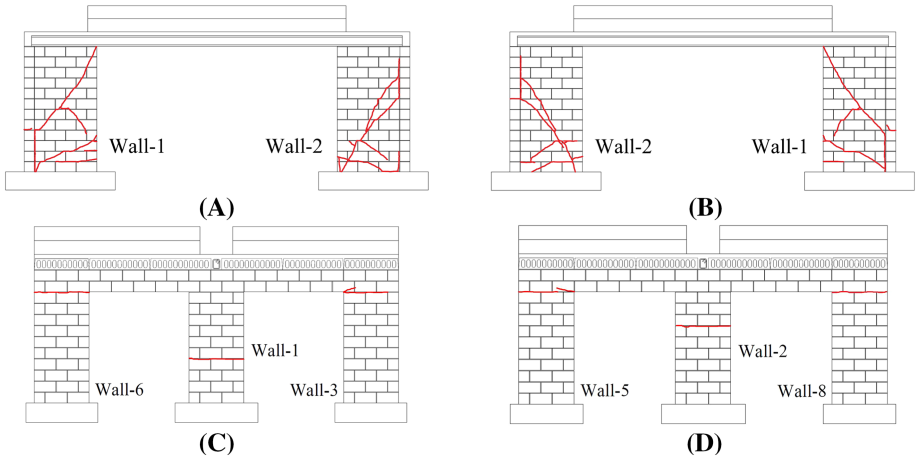

FIGURE 12 Crack patterns on Specimen 2 after MUL-160%: A, south view of two T-walls; B, north view of two T-walls; C, west view of T-wall flange and out-of-plane walls; D, east view of T-wall flange and out-of-plane walls [Colour figure can be viewed at wileyonlinelibrary.com]

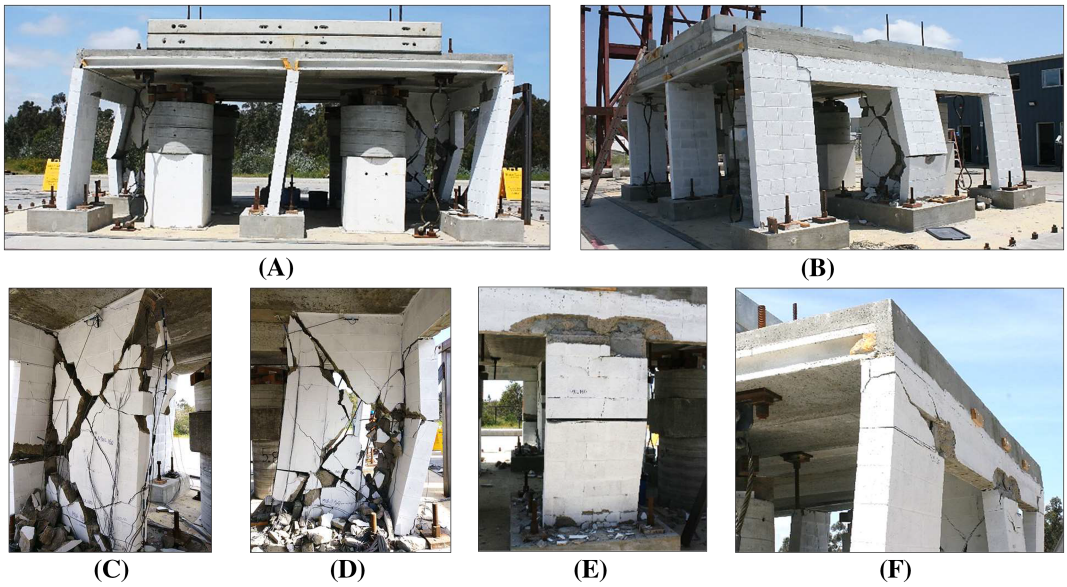

FIGURE 13 Damage in Specimen 2 after RIN-130%: A, south view of Specimen 2; B, west view of Specimen 2; C, south view of Wall 1; D, south view of Wall 2; E, damage in the flange of Wall 2; F, cracks developed near the roof and the lintels [Colour figure can be viewed at wileyonlinelibrary.com]

both walls had one vertical bar in the flange yielded at the second course from the base. No yielding was detected in the vertical bars in the webs during the last two MUL-90% tests. After the test with motion MUL-120%, most of the vertical bars in the flanges of both walls (five out of six) had yielded at the second course from the base. During the test with MUL-133%, most of the vertical and horizontal bars in the webs yielded at the locations where the major diagonal cracks developed. Yielding also occurred at the top of the extreme vertical bar near the free edge of each T-wall web. While there was no yielding detected near the top of the flange of Wall 1, two vertical bars in the flange of Wall 2 yielded near the top.

In Specimen 2, the vertical bar yielded in tension at the toe of the web of Wall 1 during test No. 2 (with MUL-90% motion), as shown in Figure 15A. In addition, the extreme vertical bar in the web of Wall 2 yielded in the region embedded in the concrete footing, indicating strain penetration. During MUL-133%, a vertical bar in the flange of Wall 2 yielded near the base. Yielding of the bars during these motions indicates that the walls were subjected to significant flexural deformation before the peak capacity was reached. During MUL-160%, with the initiation of diagonal cracks in the webs of the two T-walls, yielding occurred in the vertical and horizontal bars at locations intersected by diagonal shear cracks. Meanwhile, a few vertical bars in the wall flanges and the out-of-plane walls yielded. During the last test with RIN-130%, more bars in the webs of the T-walls yielded due to the opening of major diagonal cracks. After this test, most of the vertical bars at the top and bottom of each out-of-plane wall and T-wall flanges had yielded, showing that the walls were subjected to double-curvature bending.

The reinforcing bars in the two specimens had similar yielding sequences. Yielding first occurred in some of the vertical bars near the base of the two T-walls due to the flexural deformation. After the diagonal shear cracks opened, most of the horizontal and vertical bars in the webs of the T-walls yielded at the locations where the diagonal cracks passed. For Specimen 1, the opening of the diagonal shear cracks in the wall webs was accompanied by the yielding of the vertical bars near the top of the flange of Wall 2. For Specimen 2, yielding was detected in most of the vertical bars near the top and bottom of the T-wall flanges and the out-of-plane walls during the last ground motion test.

Figure 16 shows the locations where bar fracture occurred during the tests. In Specimen 1, fracture occurred in two horizontal bars at the locations of major diagonal crack opening during the quasi-static test. In Specimen 2, all the horizontal bars (except the two top bars) in the webs of the T-walls fractured at the locations along the major shear cracks. It can also be observed that two of the horizontal bars in Wall 1 of Specimen 2 fractured at the location of the flange–web interface due to the opening of the vertical crack at that location during MUL-160%. Moreover, the vertical bar in Wall 2 fractured near the toe. Specimen 2 had significantly more fractured bars than Specimen 1 probably because the diagonal cracks in Specimen 1 were more closely spaced, whereas in Specimen 2, the diagonal cracks were more localized inducing larger tensile strains in the horizontal bars. Furthermore, it is likely that the quasi-static pull test

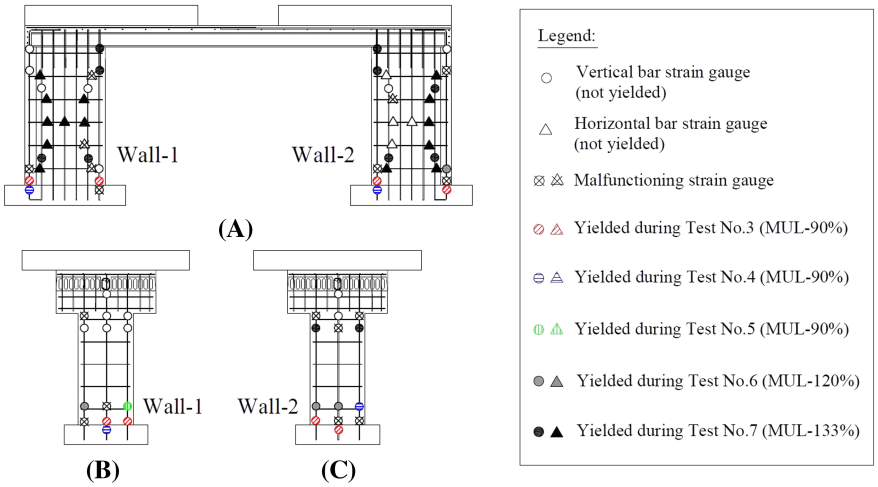

FIGURE 14 Yielding of reinforcing bars in Specimen 1: A, webs of T-walls; B, flange of Wall 1; C, flange of Wall 2

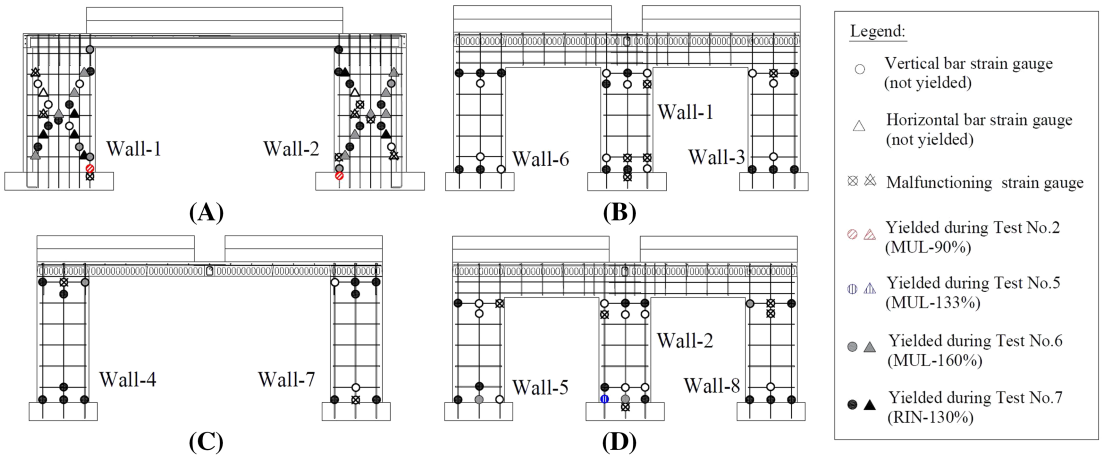

FIGURE 15 Yielding of reinforcing bars in Specimen 2: A, webs of T-walls; B, flange of Wall 1 and two west out-of-plane walls; C, two middle out-of-plane walls; D, flange of Wall 2 and two east out-of-plane walls [Colour figure can be viewed at wileyonlinelibrary.com]

conducted on Specimen 1 allowed more time for the reinforcing bars to slip, which reduced the tensile strains in the bars, when compared with a dynamic test.

7.2 | Deformation mechanism

Figure 17 shows the time histories of the drift ratios of the T-walls in the two specimens due to flexural deformation, shear deformation and wall sliding for select tests in which these walls had noticeable flexural and shear cracks. The displacement due to flexural deformation is calculated from the curvature measured by the vertical displacement transducers mounted along the two sides of each wall. The sliding displacement is the sum of the sliding measured at the top and the base of the wall by the linear potentiometers. The shear deformation is calculated by subtracting the sliding

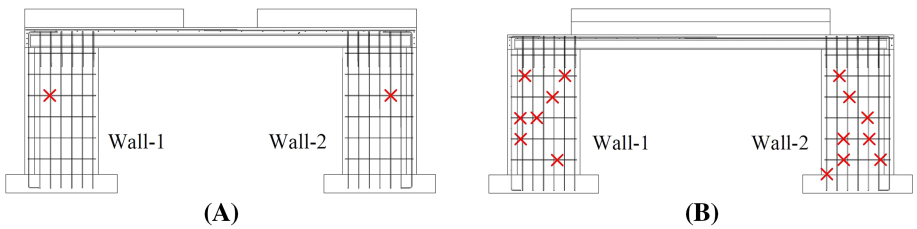

FIGURE 16 Fracture of reinforcing bars: A, Specimen 1 after the quasi-static pull test; B, Specimen 2 after RIN-130% [Colour figure can be viewed at wileyonlinelibrary.com]

and the flexural deformation from the total roof displacement. The calculated shear deformation has been checked with the data acquired by the diagonal string potentiometers. The two sets of values show good consistency. Such data were not collected in the quasi-static test of Specimen 1 because the displacement transducers had been removed. The results for Specimen 2 under RIN-130% are not shown because some of the displacement transducers got damaged during that motion.

For Specimen 1, as shown in Figure 17A, the displacement component due to flexure was significantly greater than the shear and sliding components during MUL-120. This is consistent with the flexural cracks observed and the absence of major diagonal cracks during that test, as shown in Figure 7. However, as shown in Figure 17B, during MUL-133%, the shear deformation constituted a significant portion of the total roof drift, especially after the peak roof drift had been reached, due to the opening of diagonal shear cracks. For Specimen 2, during MUL-160%, the flexural components of the two T-walls accounted for 46.9% and 63.6% of the total peak roof drift, respectively, as shown in Figure 17C. This indicates that the opening of the diagonal shear cracks was a bit delayed in Specimen 2 as compared with Specimen 1.

7.3 | Lateral Strengths

The shear strength formula of TMS 402/602[3] is used to calculate the lateral resistance of the two specimens. In this calculation, the shear–span ratio ($M_u/(V_u d_v)$) of the T-walls is taken to be 0.86 with the assumption that the walls had no rotations at the top because of the stiff roof diaphragms. Figure 18 shows that the flexural curvatures measured by the linear potentiometers at the top and the bottom of the T-walls in Specimen 1 varied in opposite directions, indicating that the walls were deformed in double curvature. However, the curvatures measured at the top of the walls were a lot smaller than those at the bottom, implying that the rigid roof diaphragm assumption was not entirely correct. The above observation has no significant consequence here because the shear–span ratio assumed is already close to the upper limit of 1.0 specified in TMS 402/602.[3] Furthermore, the axial load on each T-wall is assumed to be from the gravity load only, with the axial force introduced by the horizontal load ignored. This is a good assumption because the increase of the axial force in one wall due to the coupling effect of the roof diagonal is offset by a decrease in the other wall. The lateral resistance of Specimen 2 is assumed to be provided by the two T-walls only, and the flexural resistance of the six out-of-plane walls is ignored. The latter is relatively small. The masonry compressive strength and the yield strength of the horizontal reinforcing bars used in the calculations are based on the average values obtained from the

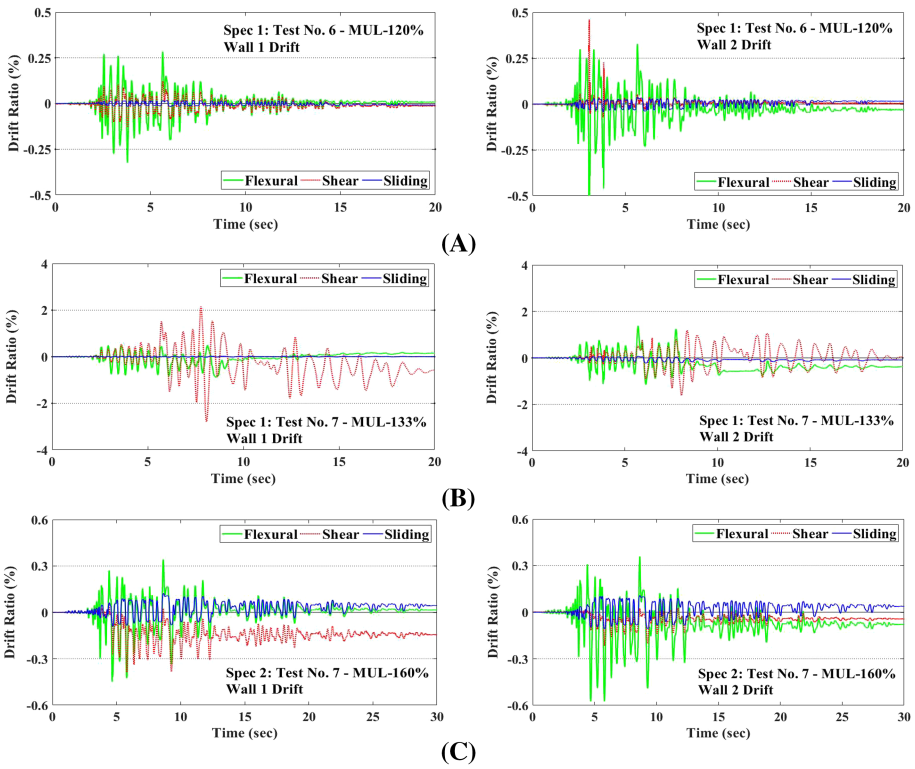

FIGURE 17 Drift time histories of the T-walls due to flexure, shear, and sliding: A, Specimen 1 during MUL-120%; B, Specimen 1 during MUL-133%; C, Specimen 2 during MUL-160% [Colour figure can be viewed at wileyonlinelibrary.com]

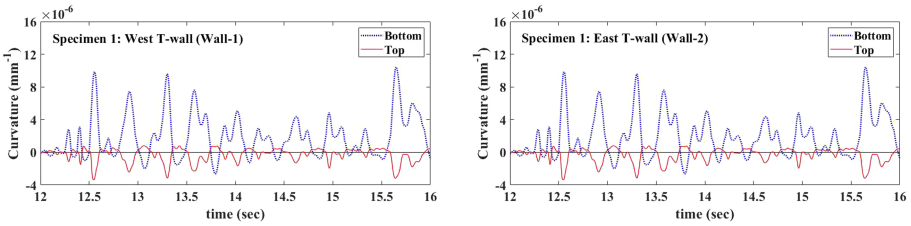

FIGURE 18 Time histories of the measured curvature near the top and bottom of two T-walls of Specimen 1 during test MUL-120%: A, west T-wall; B, east T-wall [Colour figure can be viewed at wileyonlinelibrary.com]

masonry prism tests and the tensile tests of the bars, which are shown in Tables 1 and 2. For Specimen 1, the calculated shear strength is 685 kN (154 kips), which is almost identical to the peak strength of 689 kN (155 kips) reached in the test, as shown in Figure 8. For Specimen 2, the calculated strength is 783 kN (176 kips), which is 142 kN (32 kips) lower than the peak strength reached during MUL-160%, as shown in Figure 11.

The higher lateral strength of Specimen 2, compared with Specimen 1, can be attributed to the flexural resistance and the axial restraint introduced by the six out-of-plane walls, as discussed in Mavros et al.[17] As the T-walls developed flexural deformation, they rocked on the footings because of the penetration of the tensile strains in the vertical bars into the region embedded in the footings. The rocking motion of the walls would push up the roof diaphragm, which was, however, restrained from moving up by the out-of-plane walls. Hence, the T-walls experienced increased axial compression when they rocked owing to the restraint of the out-of-plane walls. Figure 19 shows the plots of the strains in the center vertical reinforcing bars near the top of the out-of-plane walls against the roof drift during MUL-160%. It can be seen that the bars developed tension when the structure displaced in either direction. This is consistent with the flexure as well as the rocking restraint of the out-of-plane walls.

To assess the likelihood of each phenomenon, the following analyses have been conducted considering two scenarios. The results are shown in Table 6. In the first scenario, the shear resistance of the T-walls and the flexural resistance of the out-of-plane walls are calculated with the gravity load only, with the roof weight distributed among the walls in proportion to their axial stiffness. The flexural resistance of the out-of-plane walls is calculated with a fixed–fixed end condition. The total lateral resistance is the sum of the shear resistance of the T-walls and the flexural resistance of the six out-of-plane walls. In the second scenario, the rocking of the T-walls is considered, and the lateral resistance is assumed to be contributed by the shear strength of the T-walls only. In that case, the total axial compression exerted on the T-walls is calculated as the sum of the tensile forces developed by the vertical bars in the out-of-plane walls and the tributary gravity load. The tensile forces developed in the vertical bars that had not yielded during MUL-160% are calculated with the strains measured in the vertical bars near the top of each out-of-plane wall at the peak base shear. For those bars that had yielded, the average yield strength shown in Table 2 is used because the maximum tensile strains developed in those bars did not exceed the strain-hardening point. The flexural resistance of the out-of-plane walls is ignored based on the consideration that the flexural strength would diminish to zero as significant axial tension was developed in a wall. As shown in Table 6, the second scenario provides a significantly better match of the maximum lateral resistance developed in the test with a difference of only 0.3%. Hence, the higher lateral resistance of Specimen 2 is most likely due to the axial restraint of the out-of-plane walls, which is consistent to the observation of Mavros et al.[17]

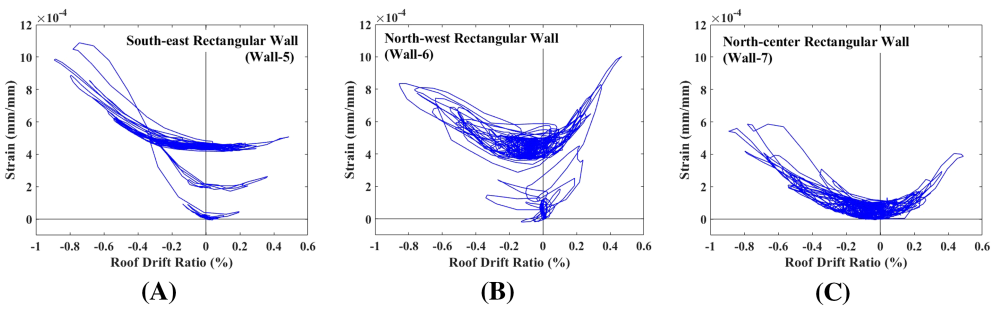

FIGURE 19 Strains in the center vertical reinforcing bars near the top of the out-of-plane walls of Specimen 2 during MUL-160% [Colour figure can be viewed at wileyonlinelibrary.com]

TABLE 6 Calculated lateral resistance of Specimen 2

	Axial load distribution 1			Axial load distribution 2		
Wall type	Wall axial load[a] [kN (kips)]	Flexural strength [kN (kips)]	Shear strength [kN (kips)]	Wall axial load[b] [kN (kips)]	Flexural strength [kN (kips)]	Shear strength [kN (kips)]
Each T-wall	126 (28.3)	431 (96.9)	393 (88.3)	409 (91.9)	599 (134.7)	464 (104.3)
Each out-of-plane wall	58 (13.0)	18 (4.0)	0	0	0	0
Base shear capacity [kN (kips)]	893 (200.8)			928 (208.6)		

[a]Tributary roof weight proportional to the wall axial stiffness.
[b]Half of the bar forces in the six out-of-plane walls plus half of the roof weight.

7.4 | Displacement capacity

Figure 20 shows the damage states of the T-walls in the two specimens when the roof drift level reached 2%, 5%, and 10%. The respective strength degradations at these drift levels can be observed from the normalized base shear–roof drift ratio curves in Figure 21. At the drift level of 2%, the strength degradation was about 25% for both specimens, and diagonal shear cracks were visible in the webs, but they were not significantly opened. Specimen 2 had more severe shear cracks, one of which propagated as a horizontal flexural crack into the flange of one T-wall. At the drift level of 5%, the strength degradation was about 50% for both specimens, and the webs of the T-walls had significant opening of the diagonal shear cracks. The webs of the T-walls in Specimen 1 exhibited severe masonry spalling, and some shear cracks propagated into the flanges. At 10% drift, the strength degradation was about 75% for both specimens, and the webs of the T-walls in both specimens had severe masonry crushing. Specimens 1 and 2 reached maximum roof drift ratios of 16.7% and 13.4%, respectively, without collapsing. At the end of the tests, the webs of the T-walls in both specimens had lost significant portions of the masonry owing to crushing, and the roof weight was carried by the wall flanges, and, for the case of Specimen 2, also by the out-of-plane walls. For Specimen 1, at the roof drift level of 16.7%, the minimum lateral resistance required to resist the P-Δ effect of the roof weight is calculated to be 41 kN (9.2 kips). This resistance could be provided by the flexural strength of the wall flanges alone, which is estimated to be 44 kN (10 kips). For Specimen 2, at the roof drift level of 13.4%, the minimum lateral resistance required to resist the P-Δ effect is calculated to be 81 kN (18 kips), while the maximum resistance that could be provided by the flexural strengths

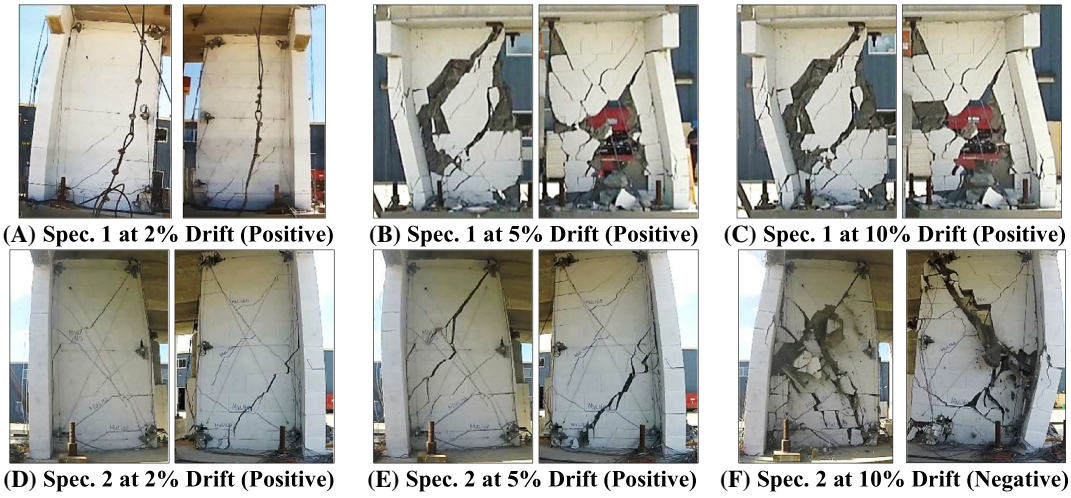

FIGURE 20 North views of the damage in the T-walls at different roof drift levels: A, Specimen 1 at 2%; B, Specimen 1 at 5%; C, Specimen 1 at 10%; D, Specimen 2 at 2%; E, Specimen 2 at 5%; F, Specimen 2 at 10% [Colour figure can be viewed at wileyonlinelibrary.com]

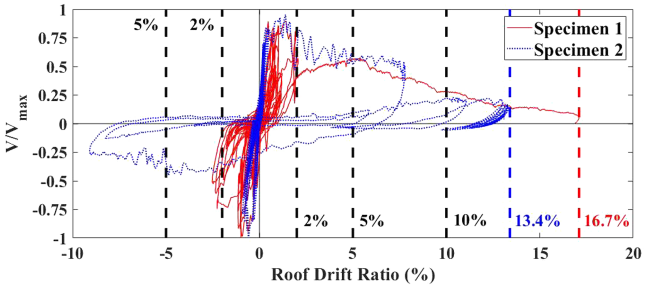

FIGURE 21 Normalized base shear–roof drift ratio curves for the test specimens [Colour figure can be viewed at wileyonlinelibrary.com]

of the flanges of the T-walls and the out-of-plane walls is calculated to be 152 kN (34 kips). At this damage state, the T-walls would not rock and the flexural strength of the out-of-plane walls could develop.

The tests have shown that RM wall systems with failure dominated by diagonal shear could develop significant lateral displacements without collapsing. The drift ratios attained and the ductility exhibited by the two specimens far exceed those observed from quasi-static tests conducted on shear-dominated planar wall segments (e.g., the tests of Voon and Ingham,[8] Shing et al.,[9,10] and Ahmadi[11]). Figures 8 and 11 compare the base shear–story drift ratio backbone curve developed by Cheng and Shing[22] on the basis of data from quasi-static wall tests to the hysteresis curves obtained from the shake-table tests. The difference in the displacement capacities is significant. The higher displacement capacity and more gentle load degradation exhibited by the shake-table test specimens can be attributed to several factors. One is the loading protocol. In typical quasi-static tests, wall specimens were normally subjected to a large number of displacement cycles with small to large amplitudes, which would introduce a more severe load degradation than what would have been experienced in an earthquake. The second is the presence of wall flanges and/or out-of-plane walls, which would carry the vertical load after the webs were severely damaged, in the shake-table test specimens, while there would be no alternative load paths for wall segments that had no flanges. However, it should be pointed out that the shake-table tests reported here had only unidirectional motion. In an earthquake, a building is subjected to excitation in multiple directions. In that case, walls oriented in different directions could suffer significant damage, and the displacement capacity of the structure will depend on the degree of damage in these walls as well as the presence or absence of gravity columns that can carry the gravity load after the vertical load carrying capacity of the walls has been depleted. Buildings with higher gravity loads could also be more vulnerable to collapse because of the more significant P-Δ effect. A recent numerical study using refined finite element models[23] has shown that one- to four-story RM archetype buildings with shear-dominated wall behavior and steel gravity frames can develop story drift ratios exceeding 10% without collapsing when subjected to bidirectional horizontal ground motions.

8 | CONCLUSIONS

This paper presents a study to investigate the collapse resistance of shear-dominated, fully grouted, RM wall systems designed for high seismic areas. Two single-story specimens, each having two RM T-walls as the seismic load resisting system, were tested on a shake table. Specimen 2 had six additional planar walls (out-of-plane walls) perpendicular to the direction of shaking. Specimen 1 was first tested with a sequence of earthquake ground motions and was finally subjected to quasi-static loading to the verge of collapse. The T-walls exhibited flexural behavior with the yielding of the vertical reinforcement during lower level earthquake motions but had failures eventually dominated by diagonal shear cracks. The maximum roof drift reached 2.52% in the ground motion tests. The maximum lateral resistance developed is close to the shear strength calculated with the formula in TMS 402/602[3] based on the assumption that the axial force in each wall is due to the gravity load only. In the quasi-static test, the roof diaphragm was pulled to a maximum drift of 16.7%, at which the lateral resistance of the wall system dropped to 6% of the peak strength; but the structure did not collapse.

Specimen 2 was tested with a sequence of earthquake ground motions up to the verge of collapse. Compared with Specimen 1, Specimen 2 had a higher lateral resistance and had first cracks observed at a higher intensity ground motion. Specimen 2 also exhibited a much lower drift ratio at comparable ground motion levels. The specimen survived the last motion without collapse. The maximum roof drift reached 13.4%, at which the residual strength dropped to 20% of the peak strength. When the shear strength of the two T-walls is calculated with the TMS 402/602[3] formula with the

consideration of the axial compression exerted by the out-of-plane walls, which restrained the rocking of the T-walls, the calculated value matches the maximum lateral resistance measured in the tests well.

The two test specimens exhibited significantly higher displacement capacities than shear-dominated planar wall segments tested in previous studies under quasi-static cyclic loads. This could be partly attributed to a smaller number of large-amplitude displacement cycles experienced by the two specimens compared with those tested under quasi-static loads. However, the higher displacement capacities can be largely attributed to the presence of wall flanges and, for the case of Specimen 2, the out-of-plane walls, which provided an alternative load path to carry the gravity load when the webs of the T-walls had been severely damaged.

RM buildings often have flanged walls and walls in different directions and may also have gravity frames, which can provide an alternative load path to carry the gravity load as well as additional axial compression on the in-plane walls when the latter rock. These systems can sustain significant lateral displacements before the P-Δ effect of the gravity load would induce collapse. In general, the displacement capacity of a building system depends on a number of factors, including the wall configuration, wall failure mechanism, presence or absence of gravity frames, the P-Δ effect of the gravity load, and the severity of wall damage induced in each direction by bidirectional earthquake ground motions. These all need to be taken into consideration to assess the collapse vulnerability of a building.

ACKNOWLEDGEMENTS

This project was supported with funding from the National Science Foundation (NSF) under Award No. CMMI-1728685. The support of the NHERI program of the NSF for the shake-table tests conducted at UC San Diego is also gratefully acknowledged. The authors are most grateful to RCP Block and Brick for their generous donation of concrete masonry units, the apprentice masons from the Brick Masons Apprenticeship Training Program of Southern California for constructing Specimen 2, and the technical staff of the Powell Structural Engineering Laboratories and the Englekirk Structural Engineering Center for their excellent support in the experimental work. The project could not have been successfully completed without the generous support of Concrete Masonry Association of California and Nevada, Masonry Institute of America, and Northwest Concrete Masonry Association. The authors would also like to thank Jeffrey Lee and Joyner Deamer, undergraduate students supported by the NSF REU program, and Richard Šusták, a visiting Master student at UC San Diego, for their assistance in test preparation. However, opinions expressed in this paper are those of the authors and do not necessarily reflect those of the sponsors.

ORCID

Jianyu Cheng https://orcid.org/0000-0002-4217-1073

REFERENCES

1. ASCE/SEI 7-16. *Minimum Design Loads for Buildings and Other Structures*. Reston, VA: ASCE; 2016.
2. FEMA. *NEHRP Quantification of Building Seismic Performance Factors*. Washington, DC: FEMA P695, Federal Emergency Agency; 2009.
3. TMS 402/602. *Building Code Requirements for Masonry Structures*. Boulder, CO: The Masonry Society; 2016.
4. Tomaževič M, Lutman M, Petković L. Seismic behavior of masonry walls: experimental simulation. *J Struct Eng*. 1996 Sep;122(9):1040-1047.
5. Sherman JD. Effects of key parameters on the performance of concrete masonry shear walls under in-plane loading. Master Thesis, Washington State University, Pullman, Washington, 2011.
6. Kapoi CM. Experimental performance of concrete masonry shear walls under in-plane loading flexure-dominated wall tests. Master Thesis, Washington State University, Pullman, Washington, 2012.
7. Shedid MT, Drysdale RG, El-Dakhakhni WW. Behavior of fully grouted reinforced concrete masonry shear walls failing in flexure: experimental results. *J Struct Eng*. 2008 Nov;134(11):1754-1767.
8. Voon KC, Ingham JM. Experimental in-plane shear strength investigation of reinforced concrete masonry walls. *J Struct Eng*. 2006 Mar; 132(3):400-408.
9. Shing PB, Schuller MP, Hoskere VS. In-plane resistance of reinforced masonry shear walls. *J Struct Eng Reston, VA*. March 1990b;116(3): 619-640.
10. Shing PB, Noland JL, Spaeh HP, Klamerus EW, Schuller MP. Response of single-story reinforced masonry shear walls to in-plane lateral loads. Department of Civil, Environmental and Architectural Engineering University of Colorado, Boulder, CO, 1991.
11. Ahmadi F. *Displacement-based seismic design and tools for reinforced masonry shear-wall structures.* Ph.D. Dissertation, Department of Civil Engineering, University of Texas at Austin, Austin, TX, 2012.
12. He L, Priestley NJ. Seismic behaviour of flanged masonry shear walls. Final report, US-Japan Coordinated Program for Masonry Building Research, Department of Applied Mechanics and Engineering Sciences, University of California San Diego, CA, USA. 1992.

13. Merryman KM, Leiva G, Antrobus N, Klingner RE. In-plane seismic resistance of two-story concrete masonry coupled shear walls, Report No. 3.1(c)-1, US-Japan Coordinated Program for Masonry Building Research, University of Texas at Austin, Austin, TX, 1990.
14. Seible F, Priestley MJ, Kingsley GR, Kürkchübasche AG. Seismic response of full-scale five-story reinforced-masonry building. *J Struct Eng*. 1994 Mar;120(3):925-946.
15. Heerema P, Shedid M, Konstantinidis D, El-Dakhakhni W. System-Level Seismic Performance Assessment of an Asymmetrical Reinforced Concrete Block Shear Wall Building. *J Struct Eng*. 2015;141(12):04015047.
16. Ashour A, El-Dakhakhni W, Shedid M. Experimental Evaluation of the System-Level Seismic Performance and Robustness of an Asymmetrical Reinforced Concrete Block Building. *J Struct Eng*. 2016;142(10):04016072.
17. Mavros M, Ahmadi F, Shing PB, Klingner RE, McLean D, Stavridis A. Shake-Table Tests of a Full-Scale Two-Story Shear-Dominated Reinforced Masonry Wall Structure. *J Struct Eng*. 2016;142(10):04016078.
18. Stavridis A, Ahmadi F, Mavros M, Shing PB, Klingner RE, McLean D. Shake-Table Tests of a Full-Scale Three-Story Reinforced Masonry Shear Wall Structure. *J Struct Eng*. 2016;142(10):04016074.
19. Tomaževič M, Weiss P. Seismic behavior of plain-and reinforced-masonry buildings. *J Struct Eng*. 1994 Feb;120(2):323-338.
20. Lourenço PB, Avila L, Vasconcelos G, Alves JP, Mendes N, Costa AC. Experimental investigation on the seismic performance of masonry buildings using shaking table testing. *Bull Earthquake Eng*. 2013 Aug 1;11(4):1157-1190.
21. Koutras A, Shing PB. Seismic behavior of a partially grouted reinforced masonry structure: shake-table testing and numerical analyses. *Earthq Eng Struct Dyn*. 2020;49(11):1115-1136.
22. Cheng J, Shing PB. Proposed Update of Nonlinear Models for Reinforced Masonry Shear Walls in ASCE 41. 11th National Conference on Earthquake Engineering, CA, 2018.
23. Koutras A. *Assessment of the seismic behavior of fully and partially grouted reinforced masonry structural systems through finite element analysis and shake-table testing*. PhD Dissertation, University of California San Diego, La Jolla, CA, 2019.
24. ASTM A615/A615M-09b. *Standard Specification for Deformed and Plain Carbon-steel Bars for Concrete Reinforcement*. West Conshohocken, PA: ASTM; 2009.
25. ACI Committee. *Building Code Requirements for Structural Concrete (ACI 318-14) and Commentary (ACI 318R-14)*. Farmington Hills, MI: American Concrete Institute; 2014.

How to cite this article: Cheng J, Koutras AA, Shing PB. Evaluation of collapse resistance of reinforced masonry wall systems by shake-table tests. *Earthquake Engng Struct Dyn*. 2020;1–20. https://doi.org/10.1002/eqe.3342